International Journal of Mechanical Sciences 161–162 (2019) 105050

Contents lists available at ScienceDirect

International Journal of Mechanical Sciences

journal homepage: www.elsevier.com/locate/ijmecsci

Low-speed impact mitigation of recoverable DNA-inspired double helical metamaterials

Jianxing Hu[a,b], T.X. Yu[c], Sha Yin[a,b], Jun Xu[a,b,*]

[a] Vehicle Energy & Safety Laboratory (VESL), Beihang University, Beijing 100191, China
[b] Department of Automotive Engineering, School of Transportation Science and Engineering, Beihang University, Beijing 100191, China
[c] Department of Mechanical & Aerospace Engineering, The Hong Kong University of Science and Technology, Clear Water Bay, Kowloon, Hong Kong

ARTICLE INFO

Keywords:
Impact mitigation
DNA-inspired metamaterials
Finite element analysis
Experiments
Spring-mass model

ABSTRACT

Metamaterials have attracted heated attention for possible impact mitigation and protection due to the outstanding mitigation capability on mechanical waves. In this study, impact mitigation of a novel metamaterials with double helixes inspired by the DNA structure is explored. The DNA-inspired double helical metamaterials (DDHM) are fabricated with the raw material of commercialized Nylon PA 2200, using an additive manufacturing machine based on selective laser sintering technology. Experiments revealed that DDHM has excellent recoverability and mitigation capability. Impact velocity, as well as the number of unit cells in DDHM chain (DDHMc) have a significant influence over the mitigation capability of DDHM. For single unit of DNA-inspired double helical metamaterials (sDDHM), mitigation rate η decreases by 21.9% from 0.251 to 0.196 within the impact velocity range from 0.35 m/s to 1.46 m/s. While for DDHMc with 5-unit cells, η decreases by 64.1% from 0.145 to 0.052 as impact velocity varied from 0.31 m/s to 1.33 m/s. Furthermore, a spring-mass model considering the nonlinear behavior is established and bandgap caused by resonance of unit cells in DDHMc is the key factor for excellent mitigation of DDHM. Results shed lights on the fundamental understanding of impact mitigation mechanism and provide useful guidelines for engineering design of impact mitigation/protection system.

1. Introduction

Impact mitigation and protection has long been a heated topic with its wide application in various sorts of industries, such as transportation [1] and architectures [2,3]. Generally, impact, crush, penetration and explosion pose great threatens to the human lives as well as to the mechanical integrity of structures [4,5].

Intuitively, most of current studies for impact protection are focused on energy absorption through large unrecoverable deformations (i.e., plastic and viscous deformations). Thanks to the discoveries of new materials [6,7] and designs [8–12] of structures, the specific energy absorption can reach up to the magnitude of 10^1 J/g [13,14]. However, in some cases, we are asked to cope with cyclic or repeated dynamic loadings. As such, a force mitigation system with recoverable structures or materials is in pressing need.

For mitigation of mechanical stress wave (induced by impact), it is critical to find ways for attenuating the peak force of blast and shock waves [15–17]. Granular-chain like materials are one form of highly efficient impact absorber by reflecting and transmitting the impact wave among granules [18–20]. In granular-chain like materials, the basic mechanism of impact mitigation is the disintegration of dispersion of waves through mass and size changes [21]. This is distinct from traditional continuum materials. Metamaterials, that possess exceptional characteristics not commonly found in natural materials, have also been employed to mitigate blast and shock wave in recent years. Tan and Khan [22,23] proposed a single-resonator model and a dual-resonator design validated by experiments to mitigate blast and shock waves, due to their unique property of negative effective mass density as a type of elastic metamaterials. Kim and Hwang [21,24,25] investigated the mitigation of nonlinear stress waves induced by impact or blast with a locally resonant woodpile metamaterials consisted of slender cylindrical rods. The above pioneering studies indicated that nonlinear contact between cylindrical rods and local resonance of rods are the key mechanism to mitigate blast and shock waves efficiently.

In recent years, the concept of bio-inspired provides an energetic perspective for metamaterials design [26–28]. Xu et al. proposed and manufactured a novel metamaterial inspired by DNA double helical structure, subsequently investigated its novel mechanical behavior with chirality [29] and mechanical logic switches based on DNA-inspired metamaterials [30]. The results demonstrated that DNA-inspired metamaterials pos-

* Corresponding author at: Department of Automotive Engineering, School of Transportation Science and Engineering, Beihang University, Beijing 100191, China.
E-mail address: junxu@buaa.edu.cn (J. Xu).

https://doi.org/10.1016/j.ijmecsci.2019.105050
Received 8 June 2019; Received in revised form 18 July 2019; Accepted 29 July 2019
Available online 29 July 2019

Nomenclature

d_c	Diameter of connecting rod (unit: mm)
d_h	Diameter of helical rod (unit: mm)
D	Diameter of a helix (unit: mm)
D_p	Diameter of lateral plate (unit: mm)
E	Elastic moduli of Nylon PA2200 (unit: GPa)
f_k	Nonlinear stiffness of mass-spring model (unit: N/m)
H	Height of DDHM (unit: mm)
κ	Wavenumber as a function of ω
m	Lumped mass of mass-spring model (unit: kg)
t_p	Thickness of lateral plate (unit: mm)
ν	Poisson's ratio of Nylon PA2200
ω	Temporal frequency of mass-spring model
ρ	Density of Nylon PA2200 (kg/m^3)
η	Mitigation rate as the ratio between maximum output acceleration and maximum input acceleration
η_{single}	Mitigation rate in single unit of DNA-inspired double helical metamaterials (sDDHM)
η_{chain}	Mitigation rate in DNA-inspired double helical metamaterials chain (DDHMc) with 5-unit cells

sess unique characteristic of an ultrabroad band gaps in low frequency domain. Therefore, it is envisioned that such metamaterials may serve as a possible excellent candidate for stress wave mitigation.

To bridge this gap, DNA-inspired metamaterials were fabricated utilizing an additive manufacturing machine (EOS P396, Germany) with selective laser sintering (SLS) technology. Subsequently, impact experiments were conducted to investigate the dynamic characteristics. Finally, a theoretical model is established to clarify the excellent mitigation mechanism of DNA-inspired metamaterials, combining with computational models validated by experiments.

2. Methodology

2.1. Metamaterials design and sample manufacturing

A DNA-inspired double helical metamaterials (DDHM) is considered in this study, the schematic of the unit cell is as sketched in Fig. 1(a). Inspired by DNA double helix structure, each unit cell consists of two cylindrical lateral plates at the ends, a double-helix part of two rods that coil around the same axis of 2π, and seven evenly-spaced connecting rods between two helical rods. Specific geometrical dimensions of the unit cell are given in Table 1.

DDHM samples were manufactured utilizing selective laser sintering (SLS) technology with an additive manufacturing machine (EOS P396, Germany), as shown in Fig. 1(b), delivering a unique advantage of manufacturing samples with complex geometry without any supporting structures [9,31]. EOS P396 system uses a pulsed laser to automatically scan cross sections of a 3D model, fusing powders and solidifying them into the designed structure layer by layer in the building platform, until the designed structure is completely finished. Typical sample fabricated as designed above is illustrated in Fig. 1(c). The raw material used here was commercialized Nylon PA 2200. All the material parameters and geometry are summarized in Table 1.

2.2. Experimental device and procedure

Impact experiments were performed in a specific testing device by design as shown in Fig. 2, as a typical Newton's cradle. The testing device contains an impactor, a hanging bar supported by two tripods and a data acquisition and recording system consisting of sensors, amplifiers and oscilloscope.

The sample was hung from the bar using 1.2 m long light string to ensure the wave propagation in the sample entirely along the horizontal axis. An impact wave was generated when the impactor released from a certain height impinged the sample, and then it propagated through the sample with a certain degree of energy dissipation. To quantify the mitigation capability, two acceleration sensors (KT10000) were attached to the lateral plates of tested sample, respectively, to record the input and output impact wave. Then the mitigation rate was found by the ratio between maximum output acceleration and maximum input acceleration. The smaller the ratio, the better the mitigation capability of the tested sample. The impact velocity can be monitored by the photogate next to the lateral plate of sample. Different impact velocities were considered by adjusting the release height of impactor. The same testing process was repeated for three times to ensure the repeatability of experiment data.

Two experimental cases, namely, a single unit of DNA-inspired double helical metamaterials (sDDHM) and a chain (DDHMc) with 5-unit cells glued together, were conducted, as shown in Fig. 3. Note that the effect of glue on the stress wave propagation can be neglected because it was extremely thin and lightweight compared to DDHMc [32].

2.3. Finite element modeling

Finite element (FE) modeling for impact tests of DDHM is conducted by using ABAQUS. To simplify, the FE model is established only with impactor and tested samples with the additional mass of 18 g coming from two sensors, neglecting the hanging bar, tripod and strings, as showed in Fig. 4. Therefore, the boundaries of samples are free at both ends.

The impactor is modeled by discrete rigid element R3D4 with the same mass and velocity as experimental cases. The samples also have the

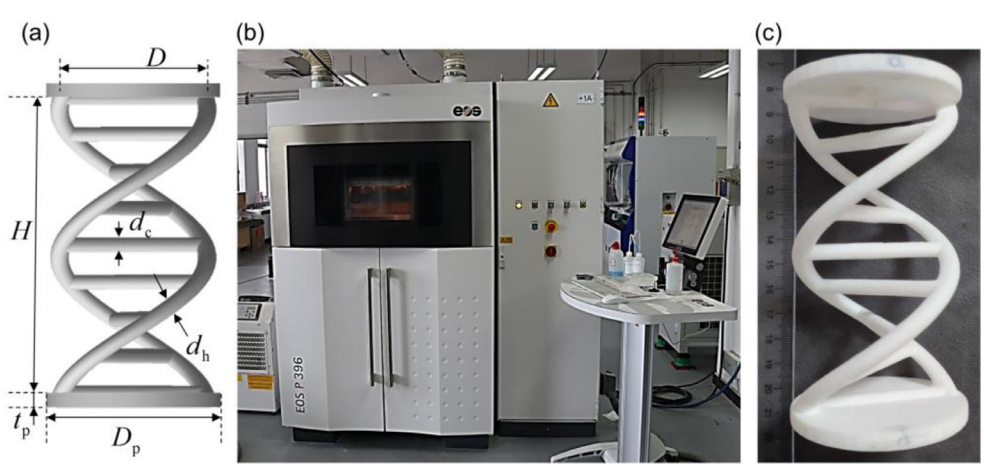

Fig. 1. Fabrication and schematic of DNA-inspired double helical metamaterials: (a) Schematics of DNA-inspired helical structure, (b) additive manufacturing equipment EOS P396, (c) schematic of 3D-printed sample.

Table 1
Geometrical dimensions and material parameters of DDHM.

Variables	Unit: mm	Nylon PA2200 [29]	
Height of DDHM, H	100	Elastic moduli, E (GPa)	1.2
Diameter of a helix, D	48	Poisson's ratio, v	0.35
Diameter of a connecting rod, d_c	5.6	Density, ρ (kg/m^3)	950
Diameter of a helical rod, d_h	5.6		
Diameter of the lateral plate, D_p	60		
Thickness of the lateral plate, t_p	10		

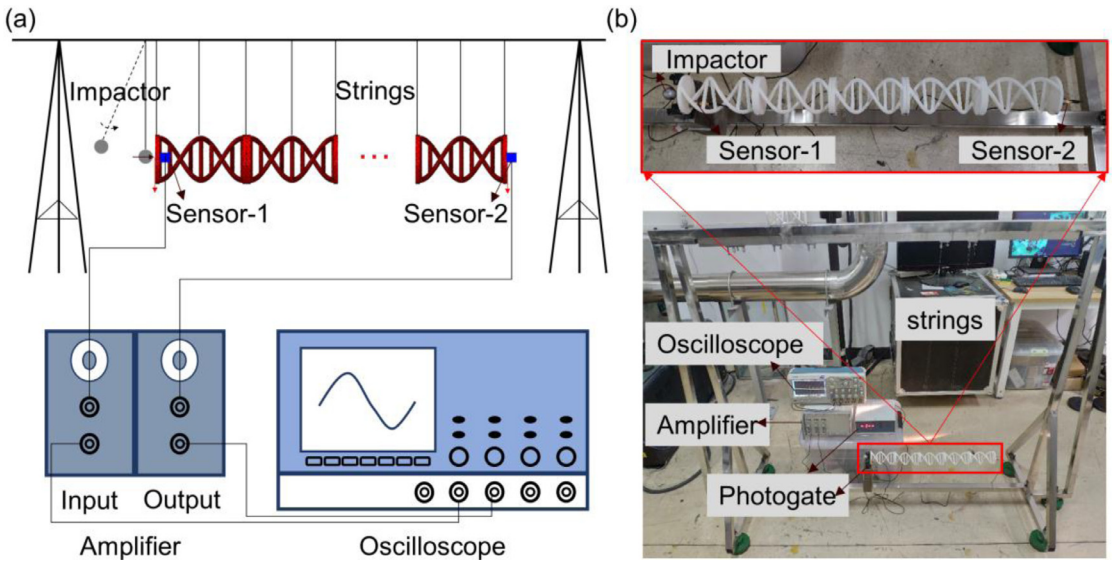

Fig. 2. Testing system used for impact experiments: (a) Schematic view with impactor impinges a sample hung by strings, then input and output waves are recorded by oscilloscope through sensors and amplifier; and (b) Experimental device with 5-unit cells.

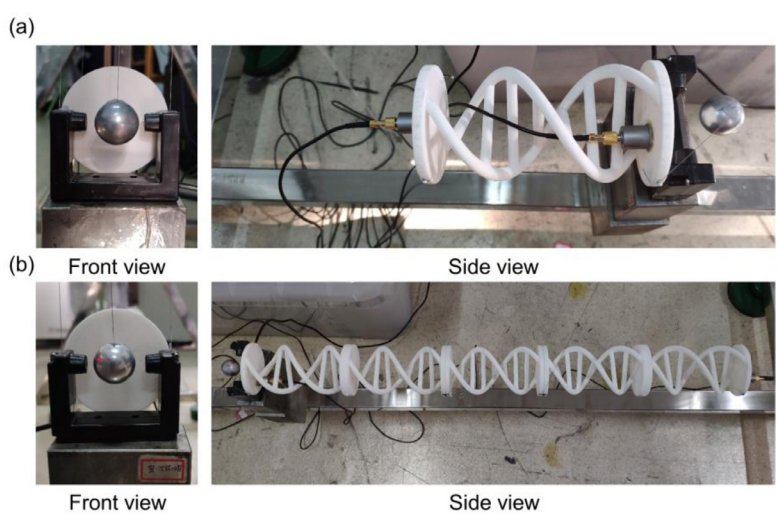

Fig. 3. Front and side views of experimental cases: (a) sDDHM and (b) DDHMc with 5-unit cells.

same dimensions as experimental conditions presented in Section 2.1, meshed using explicit 10-node quadratic tetrahedron elements C3D10M with 1.3 mm seed distribution after the analysis of convergence [29]. The element numbers of sDDHM and DDHMc cases are 15,912 and 79,560, respectively. Linear elasticity material model is adopted to describe the material property of samples. And strain rate effect is not considered due to that the material of samples will not yield in the current study. Material parameters are set as density ρ = 950 kg/m^3, Elastic modulus $E = 1.2$ GPa and Poisson's ratio $v = 0.35$, consistent with Table 1.

3. Results

3.1. Experimental result

3.1.1. sDDHM under impact velocity of 0.35 m/s

Impact tests of sDDHM under impact velocity of 0.35 m/s were conducted three times, and the computed mitigation rate between maximum output acceleration and maximum input acceleration [22,23] was found to be η = 0.247, 0.256 and 0.250, respectively (Fig. S1). Good consistency of η was obtained and the robustness and reliability of the

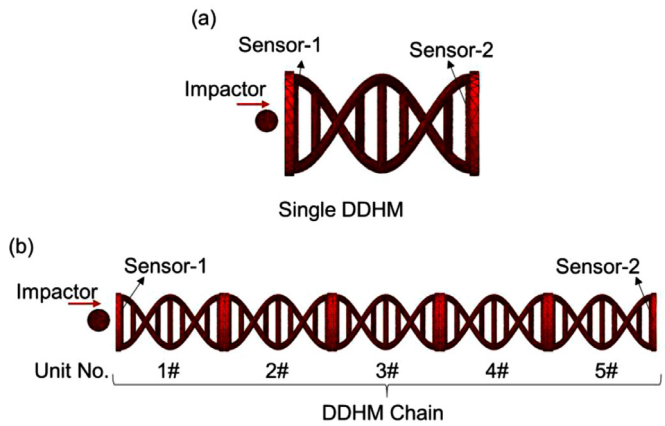

Fig. 4. Finite element models: (a) sDDHM with 15,912 C3D10M and (b) DDHMc with 79560 C3D10M.

experimental results were confirmed. For the following discussions, only one representative acceleration waveform–time curve is shown under a specific impact velocity.

Fig. 5 shows the typical input and output acceleration waveforms under impact velocity of 0.35 m/s. Impact wave attenuation could be observed for both input and output waves in Fig. 5(a). The maximum acceleration values of input and output waves were obtained from the enlarged view in Fig. 5(b), then mitigation rate η of tested sample could be computed, as $\eta = 0.256$.

3.1.2. DDHMc under impact velocity of 0.57 m/s

Typical input and output acceleration wave-time curves of a DDHMc with 5-unit cells under impact velocity of 0.57 m/s are shown in Fig. 6. More severe wave attenuation is observed in Fig. 6(a), and the mitigation rate was computed as $\eta = 0.085$. It is clear that η significantly decreases compared to sDDHM, indicating a better force mitigation capability. This is due to the fact that more energy is dissipated with increasing number of unit cells. Compared with Fig. 5(b), the number of peaks in output acceleration wave curve is reduced obviously, because the waves need to propagate a longer distance. All of this indicates that the number of unit cells in DDHMc is a critical factor, which will be discussed later utilizing the validated FE models.

3.2. Validation of finite element computation

Fig. 7 shows a good agreement of typical input and output acceleration waveform-time curves for a sDDHM under impact velocity of 0.35 m/s and a DDHMc under impact velocity of 0.57 m/s from both experimental results and numerical computations. $\eta_{\text{single}} = 0.241$ and $\eta_{\text{chain}} = 0.076$ are obtained from the computational results while the experimental values were $\eta_{\text{single}} = 0.256$ and $\eta_{\text{chain}} = 0.085$, with the deviance of 5.9% and 10.6%, respectively. In addition, it can be observed that the discrepancy between experiments and computations increases with time. This is due to reflection and transmission of waves at the interface.

Abovementioned comparative analysis between FE computations and experimental results is found to be in excellent consistent. This guarantees the validity of computational models established for impact test of DDHM.

3.3. Theoretical analysis

3.3.1. Spring-mass model

DDHMc is similar to a monoatomic chain structure [33–35] with a sequence of lumped masses connected by springs of the same stiffness. By noting that the springs here are nonlinear, a nonlinear spring-mass model is considered to describe the dispersion relation of DDHMc, as showed in Fig. 8.

The governing equation of motion of the nth lumped mass in DDHMc is expressed as follows,

$$m\ddot{u}_{\text{n}} + 2f_{\text{k}}u_{\text{n}} - f_{\text{k}}\left(u_{\text{n}-1} + u_{\text{n}+1}\right) = 0 \tag{1}$$

where m and f_{k} are lumped mass and nonlinear stiffness, respectively. After equivalent linearity of the nonlinear springs, the governing equation can be rewritten as,

$$m\ddot{u}_{\text{n}} + 2k_e u_n - k_e\left(u_{\text{n}-1} + u_{\text{n}+1}\right) = 0 \tag{2}$$

where k_{e} is equivalent stiffness. Then a harmonic wave solution can be obtained as

$$u\left(x_{\text{n}}, t\right) = u_{\text{n}}(t) = \hat{u}_{\text{n}}(\omega)e{-}^{i\omega t} = \tilde{u}(\kappa(\omega))e^{i(\kappa x\text{n}-\omega\text{t})}, \tag{3}$$

$$\hat{u}_{\text{n}}(\omega)e = \tilde{u}(\kappa(\omega))e^{i\kappa x_n} = \tilde{u}(\mu(\omega))e^{i\mu n}, \tag{4}$$

where ω and κ are temporal frequency and wave number as a function of ω.

Substituting Eq. (4) into Eq. (2) leads to

$$\left[-\omega^2 m + 2k_e - k_e\left(e^{-i\mu} + e^{i\mu}\right)\right]\tilde{u}(\mu)e^{i(\mu n-\omega t)} = 0. \tag{5}$$

To ensure Eq. (5), it requires

$$-\omega^2 m + 2k_e(1 - \cos\mu) = 0 \tag{6}$$

Thus, the dispersion relation of DDHMc is deduced as

$$\Omega^2 = 2(1 - \cos\mu),\ \Omega = \omega/\omega_e, \omega_e = \sqrt{k_e/m} \tag{7}$$

Fig. 9. portrays the dispersion curve of DDHMc obtained from Eq. (7). At the end points of the first Brillouin zone ($\mu/\pi = \pm 1$), normalized frequency Ω reaches its limiting value, which is the upper boundary

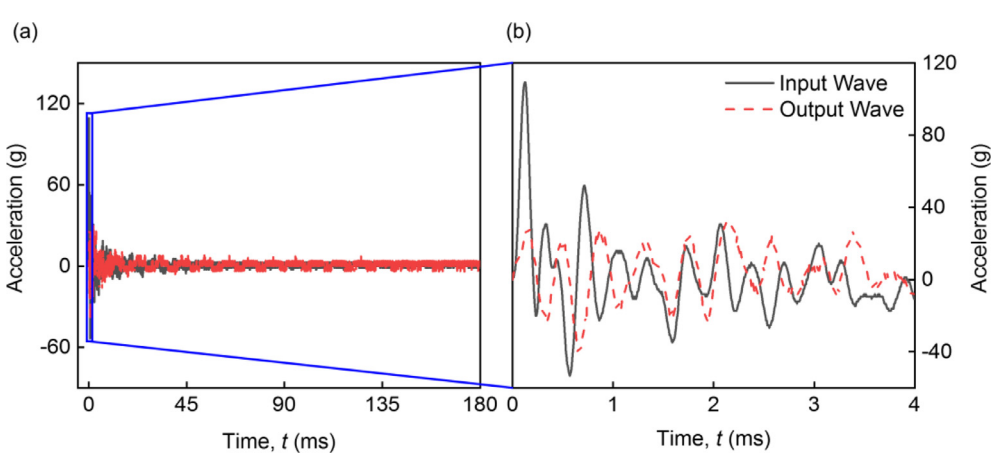

Fig. 5. Typical experimental result of a sDDHM under impact velocity of 0.35 m/s: (a) Input and output waves in time history; and (b) Enlarged view for the acceleration-time history within first 4 ms.

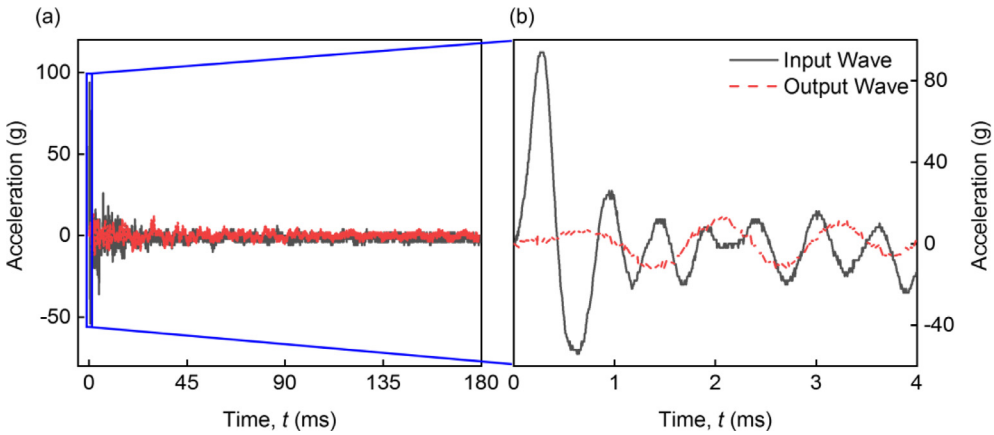

Fig. 6. Typical experimental result of a DDHM chain with 5-unit cells under impact velocity of 0.57 m/s: (a) Input and output waves in time history; and (b) Enlarged view for the acceleration-time history within first 4 ms.

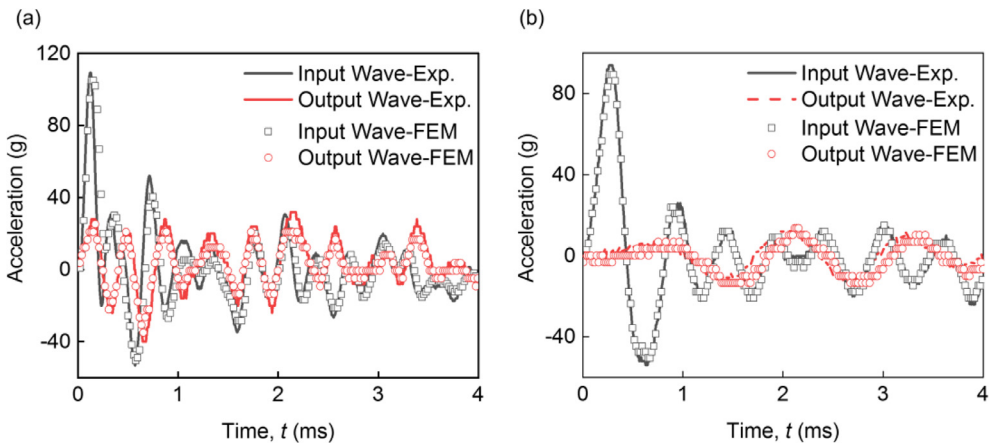

Fig. 7. Comparison between experimental and computational waves vs. time: (a) sD-DHM under impact velocity of 0.348 m/s; and (b) DDHMc with 5-unit cells under impact velocity of 0.571 m/s.

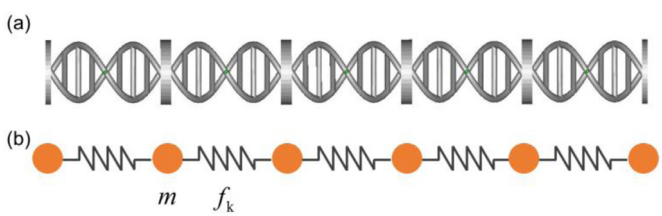

Fig. 8. (a) DDHMc with 5-unit cells, (b) nonlinear spring-mass model. Notes: m and f_k are lumped mass and nonlinear stiffness, respectively.

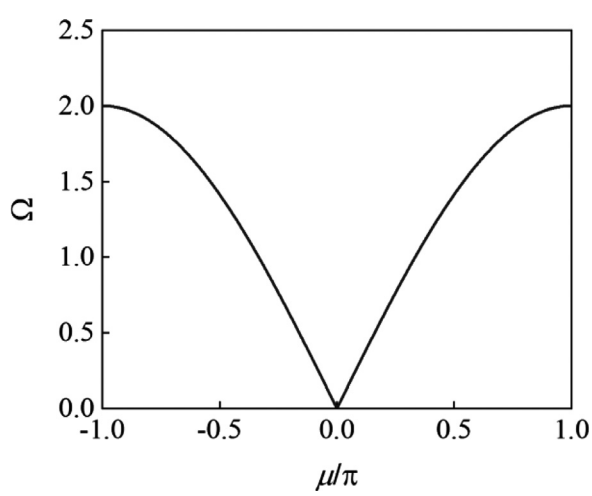

Fig. 9. Dispersion relation in the first Brillouin zone for DDHMc.

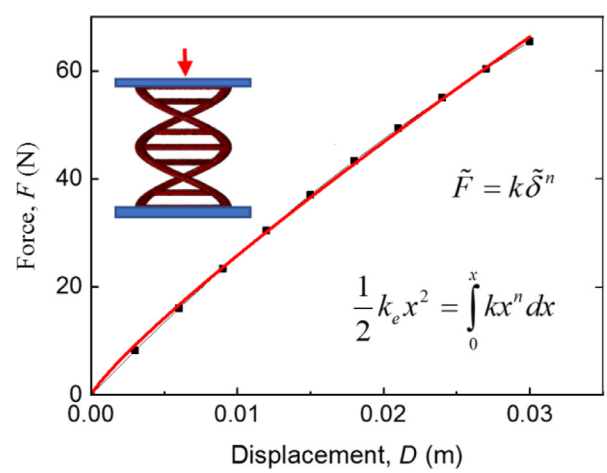

Fig. 10. Compressive force-displacement curve of DDHM to obtain the equivalent linear stiffness.

of mechanical wave propagation. Mechanical waves could not propagate through when $\Omega > 2$, i.e. a bandgap appears. On the other hand, when $0 < \Omega < 2$ mechanical waves propagate through without attenuation.

3.3.2. Mitigation mechanism analysis

Here, dispersion theory, i.e. bandgap, is applied to further clarify the mitigation mechanism of DDHMc with an excellent mitigation capability. First, the equivalent linear stiffness is obtained as $k_e = 2361$ N/m according to the potential energy equivalent in Fig. 10. Then the upper

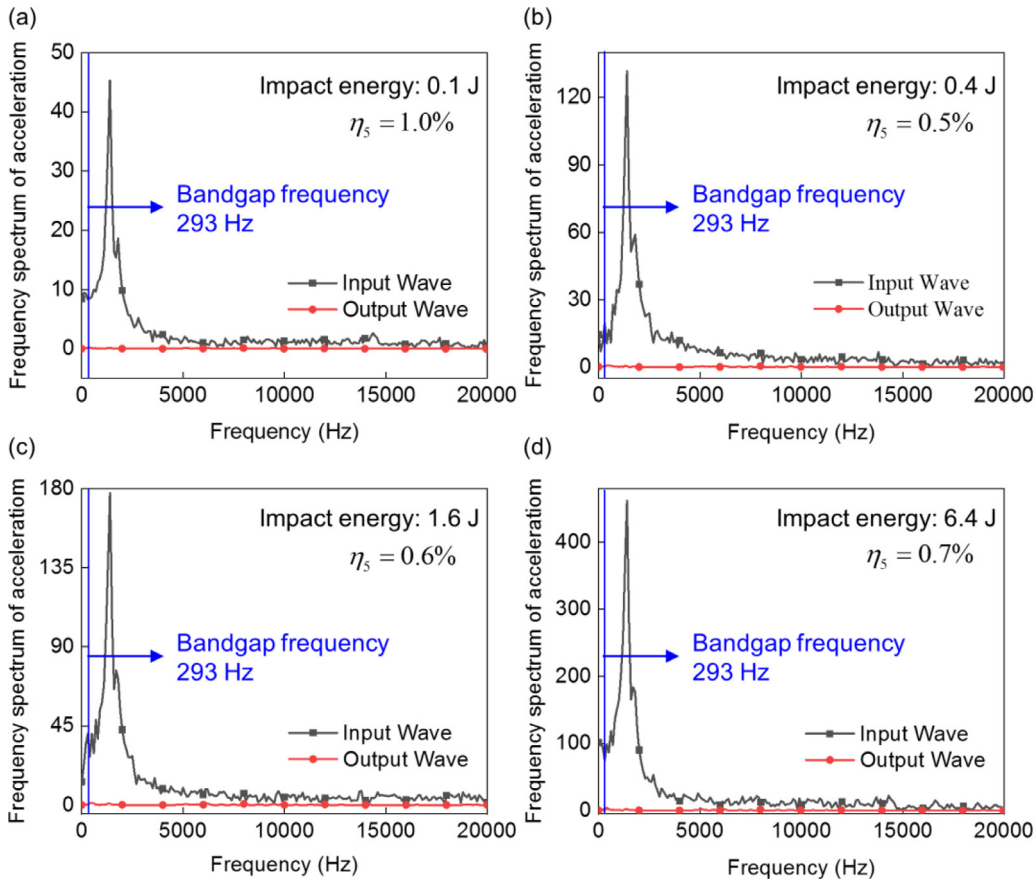

Fig. 11. FFT results of input waves under high frequency impact showing excellent impact mitigation.

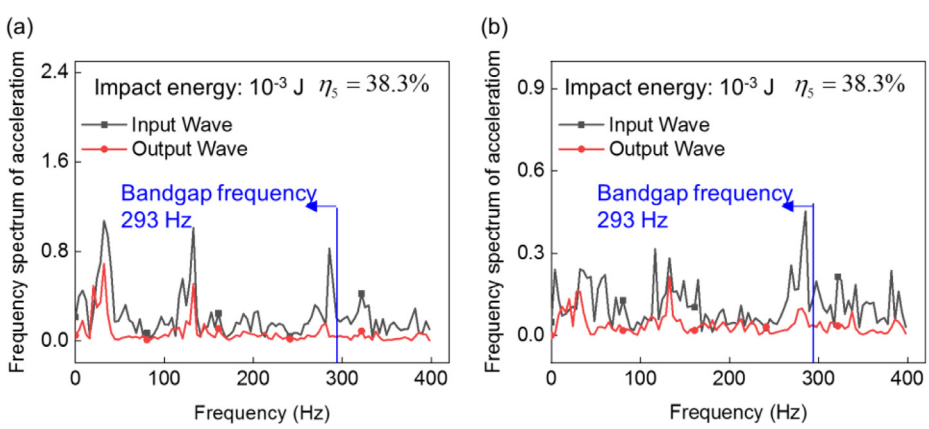

Fig. 12. FFT results of input waves under low frequency impact showing worse impact mitigation compared with high frequency impact.

boundary of mechanical wave propagation for DDHMc is computed as $f = 293$ Hz according to Eq. (7).

To validate the aforementioned analysis, impact tests with different impact energy distribution in the frequency domain are performed utilizing the validated computational models of DDHMc with 5-unit cells. And frequency domain analysis of input and output accelerations were performed to assess the attenuation of impact mitigation [36]. Fast Fourier Transform (FFT) results of input and output acceleration waves are shown in Figs. 11 and 12. It is evident that a DDHMc has an extremely outstanding mitigation capability for a high frequency impact as showed in Fig. 11. This is attributed to the fact that most of energy of initial impact waves is distributed within the bandgap frequency region (i.e. $f > 293$ Hz), such that the energy cannot propagate through. On the other hand, the mitigation capability is worsened when a DDHMc is subjected to a low frequency impact compared to high frequency impact, because in this case most impact energy is distributed in the frequency domain, capable to propagate through the DDHMc. These results indicate that the resonance of unit cells contributes to the mitigation capability of DDHMc.

4. Discussions

4.1. Influence of impact velocity

The mitigation capability under different impact velocities for both sDDHM and DDHMc with 5-unit cells is computed, as depicted in Fig. 13. For sDDHM, η decreases with impact velocity, e.g. η decreases by 21.9% from 0.251 to 0.196 within the impact velocity range of 0.35 m/s–

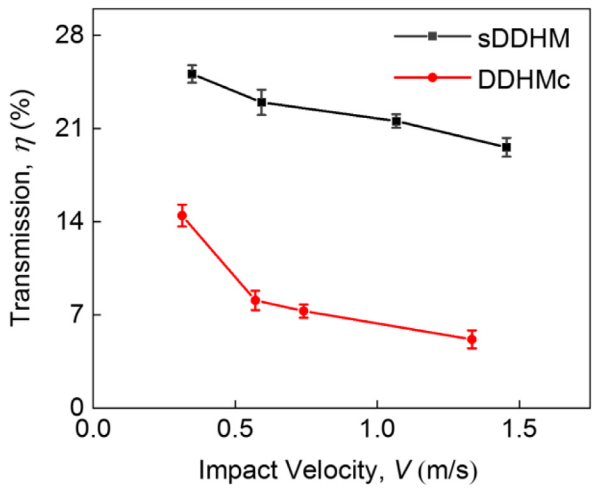

Fig. 13. Experimental results of sDDHM and DDHMc with 5-unit cells under different impact velocities.

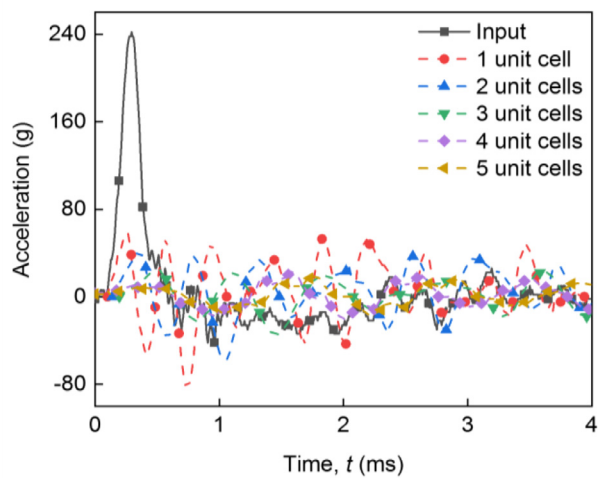

Fig. 14. Output waves of DDHMc with different unit numbers. Notes: i ($i = 1$–5) unit cells represents the output wave of DDHMc with i unit cells.

1.46 m/s. While for DDHMc, η decreases by 64.1% from 0.145 to 0.052 when impact velocity increases from 0.31 m/s to 1.33 m/s. It can be concluded, therefore, that impact mitigation of DDHM is enhanced as the impact velocity increases. This also indicates that bandgap caused by resonance of unit cells in DDHMc is extremely effective in attenuating energy of waves. As the impact velocity increases, more initial energy of impact waves is distributed in the high frequency region exceeding the bangap frequency 293 Hz, implying that more energy can be absorbed as the wave propagates through. These results provide valuable information for novel metamaterials designs applied for impact protection of materials and structures.

4.2. Influence of the number of unit cells in DDHMc

To further explore the effect of the number of unit cells on impact mitigation of DDHMc, the validated FE model of DDHMc with 5-unit cells is selected. Fig. 14 presents the computational results under impact velocity of 1.33 m/s. It is evident that the number of unit cells have a significant influence on the mitigation capability η. For quantitative comparison, η_i (subscript i represents the number of unit cells) are computed from Fig. 14 as $\eta_1 = 0.341$, $\eta_2 = 0.238$, $\eta_3 = 0.121$, $\eta_4 = 0.062$ and $\eta_5 = 0.051$. The mitigation capability of DDHMc is enhanced as the number of unit cells increases, and the enhancement becomes saturated

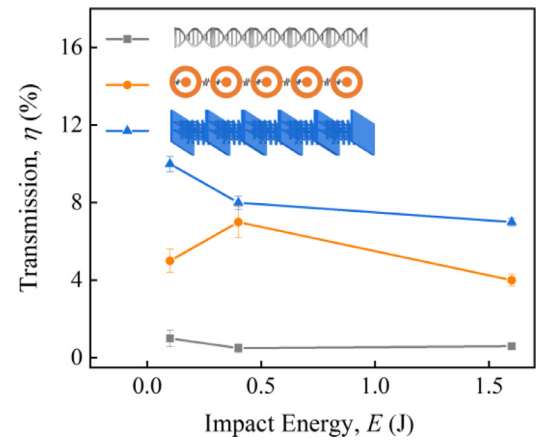

Fig. 15. Mitigation capability of DDHM compared with internal resonator metamaterials.

when the number of unit cells is more than four here. The major responsible reason should be that the initial impact energy is limited and not sufficient enough to propagate longer distance. This also means that more unit cells will be needed in DDHMc for the saturated enhancement of mitigation capability, if the initial impact energy is higher.

4.3. Mitigation capability of DDHM

Here, the mitigation capability of DDHMc was compared with internal resonator metamaterials chain (IRMc) [22,23] and sandwich-structure woodpile metamaterials [24,25] chain (SSWMc) made of Nylon PA2200 with 5-unit cells, and they have the same mass. Results in Fig. 15 show that within the impact energy range of 0.1 J–1.6 J, $\eta \approx 1\%$ for DDHMc, $\eta \approx 5\%$ for IRMc and $\eta \approx 8\%$ for SSWMc, indicating a superior force mitigation capability of the established structure. Furthermore, previous results show that DDHM has a broader bandgap attenuation compared to other reported metamaterials by Zheng and Xu [30] .

4.4. Recoverability and system stability of DDHM

Recoverability is also a major advantage of DDHM, in addition to the excellent mitigation capability. Here, the loading-unloading curves of sDDHM are used to demonstrate the recoverability in Fig. 16. Sample is recovered up to 98% of their original height with compression strain of 30% after unloading, while the residual deformation can be explained by anelasticity of nylon material, which can be gradually recovered once loading is removed and fully recovered after 5 min as shown in Fig. 16(b). The results indicate that DDHM is a recoverable metamaterials with the ability to cope with cyclic or repeated dynamic loadings.

In the meantime, note that stability problems of sDDHM and DDHMc, as 1D structures, would likely occur if the ratio between the height of DDHM (H) and diameter of a helix (D) is too large or a chain has too many unit cells. The stability of DDHM cannot be simply described by the Euler buckling theory and more complicated stability analysis of helical rod need to be considered [37–39]. Liu et al. found that there are some differences between the Euler's and Lyapunov's stability concepts of helical equilibrium and the tangential force for the Lyapunov's stability in time domain is larger than Euler's critical load [38]. In addition, it is possible to extend DDHM to 2D and 3D structures to avoid instability of DDHM. One way is to add DDHM unit cells along 2 and 3 directions for forming 2D and 3D metastructures, which possess excellent mitigation capability under more sophisticated impacting scenarios. This possibility will be investigated in our future work.

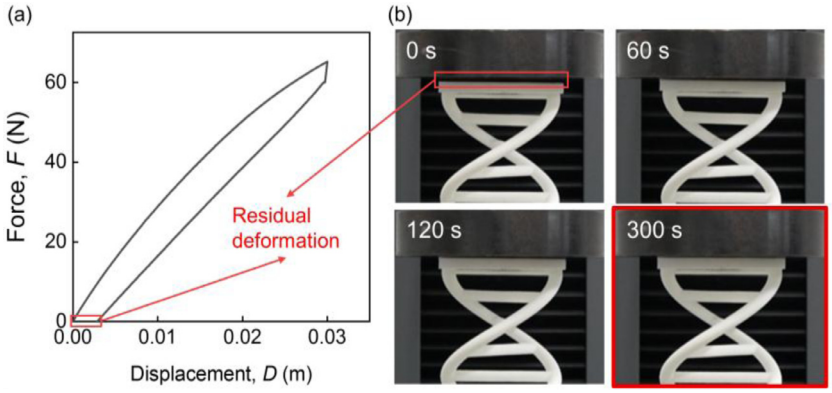

Fig. 16. (a) Force-displacement curves of sDDHM under one cyclic loading with relative compression displacement of 30%; (b) Recovery of sample after unloading completely.

5. Concluding remarks

Impact mitigation of DNA-inspired double helical metamaterials (DDHM) is investigated systematically. Both DDHM cell and chain share an excellent mitigation characteristic. Furthermore, a nonlinear spring-mass model reveals that bandgap caused by resonance of unit cells in DDHMc serving as the critical mitigation mechanism. By using the mitigation rate η, which is defined as the ratio between maximum output acceleration and maximum input acceleration, to quantitatively evaluate the mitigation capability of DDHM, it is revealed that the number of unit cells in DDHMc and impact velocity of the impactor have significant influences on the mitigation capability of DDHMc.

In the current study, nylon is used to fabricate the structure such that it cannot withstand large impact energy. Also, we only focuses on the impact mitigation (one-time impact) of the DDHM, the repeated impacts and durability of the system will be discussed in the future. Nonetheless, the results of this study pave a way for future design and manufacturing of the novel bionic metamaterials for stress wave mitigation and provide a guideline for proper design of metamaterials and metastructures for possible engineering applications.

Supplementary materials

Supplementary material associated with this article can be found, in the online version, at doi:10.1016/j.ijmecsci.2019.105050.

References

[1] Xu J, Li YB, Chen X, Ge DY, Liu BH, Zhu MY, Park TH. Automotive windshield — pedestrian head impact: energy absorption capability of interlayer material. Int J Auto Tech 2011;12:687.
[2] Luccioni BM, Ambrosini RD, Danesi RF. Analysis of building collapse under blast loads. Eng Struct 2004;26:63–71.
[3] Yuan SJ, Hao H, Zong ZH, Li J. A study of RC bridge columns under contact explosion. Int J Impact Eng 2017;109:378–90.
[4] Deans GT, Magalliard JN, Kerr M, Rutherford WH. Neck sprain—a major cause of disability following car accidents. Injury-Int J Care Inj 1987;18:10–12.
[5] Yin S, Li J, Xu J. Exploring the mechanisms of vehicle front-end shape on pedestrian head injuries caused by ground impact. Accid Anal Prev 2017;106:285–96.
[6] Jia Z, Yu Y, Hou S, Wang L. Biomimetic architected materials with improved dynamic performance. J Mech Phys Solids 2019;125:178–97.
[7] Sun Y, Guo Z, Xu J, Xu X, Liu C, Li Y. A candidate of mechanical energy mitigation system: dynamic and quasi-static behaviors and mechanisms of zeolite beta/water system. Mater Des 2015;66:545–51.
[8] Ha NS, Lu GX, Xiang XM. High energy absorption efficiency of thin-walled conical corrugation tubes mimicking coconut tree configuration. Int J Mech Sci 2018;148:409–21.
[9] Yin S, Li J, Chen H, Robert O R, Xu J. Design and strengthening mechanisms in hierarchical architected materials processed using additive manufacturing. Int J Mech Sci 2018;149:150–63.
[10] Hu J, Lu G, Yang H, Yu TX, Xu J. Dynamic response of internally nested hemispherical shell system to impact loading. Thin Wall Struct 2017;120:29–37.
[11] Tan X, Chen S, Zhu S, Wang B, Xu P, Yao K, Sun Y. Reusable metamaterial via inelastic instability for energy absorption. Int J Mech Sci 2019;155:509–17.
[12] Zhang J, Karagiozova D, You Z, Chen Y, Lu G. Quasi-static large deformation compressive behaviour of origami-based metamaterials. Int J Mech Sci 2019;153:194–207.
[13] Hu J, Yin S, Yu TX, Xu J. Dynamic compressive behavior of woven flax-epoxy-laminated composites. Int J Impact Eng 2018;117:63–74.
[14] Hussein RD, Ruan D, Lu GX, Guillow S, Yoon JW. Crushing response of square aluminium tubes filled with polyurethane foam and aluminium honeycomb. Thin Wall Struct 2017;110:140–54.
[15] Hu D, Hu J, Jiang H, Xu J. A highly effective energy mitigation system combining carbon nanotube and buckyballs. Eur Phys J-Spec Top 2018;227:155–66.
[16] Xu J, Hu R, Chen X, Hu D. Impact protection behavior of a mordenite zeolite system. Eur Phys J-Spec Top 2016;225:363–73.
[17] Xu J, Li Y, Xiang Y, Chen X. A super energy mitigation nanostructure at high impact speed based on buckyball system. PLoS ONE 2013;8:e64697.
[18] Carretero-Gonzlez A acute R, Khatri D, Porter MA, Kevrekidis PG, Daraio C. Dissipative solitary waves in granular crystals. Phys Rev Lett 2009;102:024102.
[19] Daraio C, Nesterenko VF, Herbold EB, Jin S. Energy trapping and shock disintegration in a composite granular medium. Phys Rev Lett 2006;96:058002.
[20] Hong J. Universal power-law decay of the impulse energy in granular protectors. Phys Rev Lett 2005;94:108001.
[21] Kim E, Yang J, Hwang H, Shul CW. Impact and blast mitigation using locally resonant woodpile metamaterials. Int J Impact Eng 2017;101:24–31.
[22] Khan MH, Li B, Tan KT. Impact load wave transmission in elastic metamaterials. Int J Impact Eng 2018;118:50–9.
[23] Tan KT, Huang HH, Sun CT. Blast-wave impact mitigation using negative effective mass density concept of elastic metamaterials. Int J Impact Eng 2014;64:20–9.
[24] Kim E, Yong HNK, Yang J. Nonlinear stress wave propagation in 3D woodpile elastic metamaterials. Int J Solids Struct 2015;58:128–35.
[25] Hwang H, Lee J, Yang J, Shul C, Kim E. Sandwich-structured woodpile metamaterials for impact mitigation. Int J Appl Mech 2018;10(7):1850078.
[26] Chen Y, Wang L. Multiband wave filtering and waveguiding in bio-inspired hierarchical composites. Extreme Mech Lett 2015;5:18–24.
[27] Chen Y, Wang L. Bio-inspired heterogeneous composites for broadband vibration mitigation. Sci Rep 2015;5:17865.
[28] Miniaci M., Krushynska A., Movchan A.B., Bosia F., Pugno N.M. Spider-web inspired mechanical metamaterials. 2016.
[29] Zheng B, Liu Y, Liu J, Yin S, Xu J. Novel mechanical behaviors of DNA-inspired helical structures with chirality. Int J Mech Sci 2019;161-162:105025.
[30] Zheng B, Xu J. Mechanical logic switches based on DNA-inspired acoustic metamaterials with ultrabroad low-frequency band gaps. J Phys D Appl Phys 2017;50:465601.
[31] Xu J, Wu Y, Wang L, Li J, Yang Y, Tian Y, Gong Z, Zhang P, Nutt S, Yin S. Compressive properties of hollow lattice truss reinforced honeycombs (Honeytubes) by additive manufacturing: patterning and tube alignment effects. Mater Des 2018;156:446–57.
[32] Dong XL, Gao ZY, Yu TX. Dynamic crushing of thin-walled spheres: an experimental study. Int J Impact Eng 2008;35:717–26.
[33] Amendola A, Krushynska A, Daraio C, Pugno NM, Fraternali F. Tuning frequency band gaps of tensegrity mass-spring chains with local and global prestress. Int J Solids Struct 2018;155:47–56.
[34] Krushynska AO, Amendola A, Bosia F, Daraio C, Pugno NM, Fraternali F. Accordion-like metamaterials with tunable ultra-wide low-frequency band gaps. New J Phys 2018;20:073051.
[35] Slepyan L, Cherkaev A, Cherkaev E. Transition waves in bistable structures. II. Analytical solution: wave speed and energy dissipation. J Mech Phys Solids 2005;53:407–36.
[36] Song B, Nelson K. Dynamic characterization of frequency response of shock mitigation of a Polymethylene Diisocyanate (PMDI) based rigid polyurethane foam. Lat Am J Solids Stru 2015;12:1790–806.
[37] Y-z Liu, Y Xue. Stability analysis of helical rod based on exact cosserat model. Appl Math Mech-Engl 2011;32:603–12.
[38] Liu Y, Sheng L. Stability and vibration of a helical rod constrained by a cylinder. Acta Mech Sin 2007;23:215–19.
[39] Zhou ZC, Lai PY, Joos B. Elasticity and stability of a helical filament. Phys Rev E 2005;71.